JCI insight

Altered calcium handling produces reentry-promoting action potential alternans in atrial fibrillation–remodeled hearts

Tao Liu, … , Congxin Huang, Stanley Nattel

Research Article **Cardiology**

Atrial fibrillation (AF) alters atrial cardiomyocyte (ACM) Ca^{2+} handling, promoting ectopic beat formation. We examined the effects of AF-associated remodeling on Ca^{2+}-related action potential dynamics and consequences for AF susceptibility. AF was maintained electrically in dogs by right atrial (RA) tachypacing. ACMs isolated from AF dogs showed increased Ca^{2+} release refractoriness, spontaneous Ca^{2+} spark frequency, and cycle length (CL) threshold for Ca^{2+} and action potential duration (APD) alternans versus controls. AF increased the in situ CL threshold for Ca^{2+}/APD alternans and spatial dispersion in Ca^{2+} release recovery kinetics, leading to spatially discordant alternans associated with reentrant rotor formation and susceptibility to AF induction/maintenance. The clinically available agent dantrolene reduced Ca^{2+} leak and CL threshold for Ca^{2+}/APD alternans in ACMs and AF dog right atrium, while suppressing AF susceptibility; caffeine increased Ca^{2+} leak and CL threshold for Ca^{2+}/APD alternans in control dog ACMs and RA tissues. In vivo, the atrial repolarization alternans CL threshold was increased in AF versus control, as was AF vulnerability. Intravenous dantrolene restored repolarization alternans threshold and reduced AF vulnerability. Immunoblots showed reduced expression of total and phosphorylated ryanodine receptors and calsequestrin in AF and unchanged phospholamban/SERCA expression. Thus, along with promoting spontaneous ectopy, AF-induced Ca^{2+} handling abnormalities favor AF by enhancing vulnerability to repolarization alternans, promoting initiation and maintenance of reentrant activity; dantrolene provides a lead […]

Find the latest version:

https://jci.me/133754/pdf

JCI insight

Altered calcium handling produces reentry-promoting action potential alternans in atrial fibrillation–remodeled hearts

Tao Liu,[1,2,3,4] Feng Xiong,[1,5] Xiao-Yan Qi,[1] Jiening Xiao,[1] Louis Villeneuve,[1] Issam Abu-Taha,[6] Dobromir Dobrev,[6] Congxin Huang,[2,3,4] and Stanley Nattel[1,5,6,7]

[1]Montreal Heart Institute, Department of Medicine, Université de Montréal, Montréal, Québec, Canada. [2]Department of Cardiology, Renmin Hospital of Wuhan University, China. [3]Cardiovascular Research Institute, Wuhan University, China. [4]Hubei Key Laboratory of Cardiology, Wuhan, China. [5]Department of Pharmacology and Therapeutics, McGill University, Montréal, Québec, Canada. [6]Institute of Pharmacology, West German Heart and Vascular Center, Faculty of Medicine, University Duisburg-Essen, Germany. [7]IHU LIRYC Institute, Fondation Bordeaux Université, Bordeaux, France.

Atrial fibrillation (AF) alters atrial cardiomyocyte (ACM) Ca^{2+} handling, promoting ectopic beat formation. We examined the effects of AF-associated remodeling on Ca^{2+}-related action potential dynamics and consequences for AF susceptibility. AF was maintained electrically in dogs by right atrial (RA) tachypacing. ACMs isolated from AF dogs showed increased Ca^{2+} release refractoriness, spontaneous Ca^{2+} spark frequency, and cycle length (CL) threshold for Ca^{2+} and action potential duration (APD) alternans versus controls. AF increased the in situ CL threshold for Ca^{2+}/APD alternans and spatial dispersion in Ca^{2+} release recovery kinetics, leading to spatially discordant alternans associated with reentrant rotor formation and susceptibility to AF induction/ maintenance. The clinically available agent dantrolene reduced Ca^{2+} leak and CL threshold for Ca^{2+}/ APD alternans in ACMs and AF dog right atrium, while suppressing AF susceptibility; caffeine increased Ca^{2+} leak and CL threshold for Ca^{2+}/APD alternans in control dog ACMs and RA tissues. In vivo, the atrial repolarization alternans CL threshold was increased in AF versus control, as was AF vulnerability. Intravenous dantrolene restored repolarization alternans threshold and reduced AF vulnerability. Immunoblots showed reduced expression of total and phosphorylated ryanodine receptors and calsequestrin in AF and unchanged phospholamban/SERCA expression. Thus, along with promoting spontaneous ectopy, AF-induced Ca^{2+} handling abnormalities favor AF by enhancing vulnerability to repolarization alternans, promoting initiation and maintenance of reentrant activity; dantrolene provides a lead molecule to target this mechanism.

Introduction

Atrial fibrillation (AF), the most common sustained cardiac arrhythmia in clinical practice, is associated with significant morbidity and mortality (1). AF prevalence is age dependent and will continue to rise as the population ages (1). Current therapeutic approaches for AF face limitations related to suboptimal efficacy and adverse effect potential; new insights into underlying mechanisms might help identify novel therapeutic strategies (2).

AF-associated remodeling has long been known to alter atrial Ca^{2+} handling (3). The rapid atrial rates associated with AF produce early cellular Ca^{2+} loading (4), followed by changes in cell Ca^{2+} handling that reduce the systolic Ca^{2+} transient while causing marked hypocontractility (3). One curious finding in such remodeled cardiomyocytes is that although the steady-state Ca^{2+} transient during sustained activity is very small, the initial transient after a period of inactivity is nearly normal (3). One possible explanation would be an alteration in refractoriness of the Ca^{2+} transient. Prolonged Ca^{2+} transient refractoriness (CTR) decreases Ca^{2+} transients with repeated activation, especially at rapid rates, and increases susceptibility to alternans behavior (5).

Abnormalities in cardiac ryanodine receptor (RyR2) function are well known to occur in AF and are associated with aberrant Ca^{2+} releases that cause delayed afterdepolarizations, triggered activity, and spontaneous ectopic firing (6–9). In a mouse knockin model harboring a "leaky" RyR2 (RyR2 R2474S), Xie et al. found increased susceptibility to atrial cardiomyocyte action potential (AP) alternans and atrial arrhythmias (10). A computational study suggested that disrupted Ca^{2+} release induced by impaired RyR2 inac-

tivation might promote atrial alternans and arrhythmia susceptibility in patients with AF (11); however, there has been no direct demonstration.

We speculated that abnormal Ca^{2+} handling associated with AF might increase CTR and that Ca^{2+} handling disturbances might not only predispose to abnormal Ca^{2+} releases, causing spontaneous atrial ectopic activity, but also promote alternans behavior and susceptibility to reentry. We assessed this possibility in a dog model of electrically maintained AF, with a combination of cellular Ca^{2+} imaging, simultaneous tissue optical Ca^{2+}/transmembrane potential (Vm) optical mapping, and in vivo electrophysiology. Our results suggest that AF-associated Ca^{2+} handling disturbances may be central not only to the trigger for reentry in terms of ectopic beat formation but also to the substrate for reentry through enhanced susceptibility to AP alternans.

Results

AF-related changes in CTR and Ca^{2+} release restitution. Figure 1A shows representative recordings of cytosolic Ca^{2+} transients (CaTs) at various S1-S2 coupling intervals from each group. AF prolonged CTR, which averaged 197 ± 13 ms in AF atrial cardiomyocytes (ACMs) versus 144 ± 7 ms in CTLs ($P < 0.01$; Figure 1B). Figure 1C shows typical CaT restitution curves, fitted by monoexponential relationships. AF increased the steepness of CaT restitution, decreasing the restitution time constant (τ) from 591 ± 18 ms in CTL ACMs to 315 ± 13 ms ($P < 0.001$; Figure 1D).

Changes in the threshold for cellular CaT alternans. It has long been recognized that changes in $[Ca^{2+}]_i$ are central to the development of repolarization alternans (12). Figure 2A shows cellular CaT recordings at progressively higher frequencies. In each case, beat-to-beat CaT alternans eventually appeared. The threshold frequency for alternans in each ACM in each group is shown in Figure 2B. The CaT alternans frequency threshold was significantly reduced, by 40%, in AF ACMs.

Changes in CaT and sarcoplasmic reticulum Ca^{2+} content. The results in Figure 1 and Figure 2 show that Ca^{2+} release dynamics are altered in AF ACMs. To relate these changes in dynamics to basic Ca^{2+} handling properties, we determined the effects of AF on CaT properties and sarcoplasmic reticulum (SR) Ca^{2+} content under fixed-rate pacing. Supplemental Figure 1A (supplemental material available online with this article; https://doi.org/10.1172/jci.insight.133754DS1) shows representative CaT recordings. Diastolic $[Ca^{2+}]_i$ was increased, while CaT amplitude was significantly decreased, in AF ACMs (Supplemental Figure 1B). Changes in SR Ca^{2+} content were assessed by simultaneously measuring caffeine-induced CaTs and sodium-calcium exchange (NCX) currents. Supplemental Figure 2A shows representative recordings of caffeine-induced CaTs and NCX currents from CTL and AF ACMs. AF significantly increased caffeine-induced NCX current amplitude and SR Ca^{2+} content (Supplemental Figure 2, B and C) without affecting $[Ca^{2+}]_i$ decay kinetics (Supplemental Figure 2D).

Changes in spontaneous Ca^{2+} spark and spontaneous CaT events. To relate spontaneous RyR2 release behavior to changes in alternans, we quantified spontaneous Ca^{2+} spark (SCaS) cellular events with confocal microscopy and Ca^{2+} microfluometry. Figure 3A shows original 2-dimensional snapshots of $[Ca^{2+}]_i$ fluorescence from each group. Data for SCaS frequency, Ca^{2+} spark–mediated leak, Ca^{2+} spark area, Ca^{2+} spark amplitude, and Ca^{2+} spark mass in all ACMs are compared in Figure 3, B–F. SCaS frequency and Ca^{2+} spark–mediated leak were significantly increased in AF ACMs versus CTLs (SCaS frequency: 6.5 ± 0.4/1000 $\mu m^2 \times s$ in AF vs. 1.2 ± 0.1/1000 $\mu m^2 \times s$ in CTLs, Figure 3B; Ca^{2+} spark–mediated leak: 8.9 ± 0.9 $\Delta F/F0/1000$ s in AF vs. 1.3 ± 0.2 $\Delta F/F0/1000$ s in CTL, Figure 3C; $P < 0.001$ for each). There was no significant difference in Ca^{2+} spark area (Figure 3D), Ca^{2+} spark amplitude (Figure 3E), or Ca^{2+} spark mass (Figure 3F) between CTL and AF ACMs. We also recorded spontaneous CaT (SCaT) events after a 30-second period of pacing at 2 Hz. Compared with CTL ACMs, more SCaTs were seen in AF cells after the cessation of cell stimulation (6.3 ± 0.5 in AF vs. 1.7 ± 0.3 in CTLs, $P < 0.001$; Supplemental Figure 3).

In situ alterations in atrial Ca^{2+} handling dynamics and heterogeneity. To relate AF-induced single-ACM changes to cellular alterations in intact tissue, we performed optical $[Ca^{2+}]_i$ mapping in coronary-perfused canine atrial preparations. Figure 4A shows typical maps of S2/S1 CaT ratio at 4 S1-S2 coupling intervals. The S2/S1 CaT ratio was significantly decreased at all coupling intervals below 220 ms in AF atria compared with CTLs (all $P < 0.001$; Figure 4B), corresponding to the single-ACM results (Figure 1). However, in situ mapping revealed an additional effect of AF: a marked increase in regional variability with premature activation (Figure 4A). Spatial CaT inhomogeneity was quantified as the coefficient of variation (COV) of S2/S1 CaT ratio (COV ratio). The COV ratio was strikingly increased in AF atria, with significant changes at all coupling intervals below 240 ms compared with CTLs ($P < 0.001$; Figure 4C).
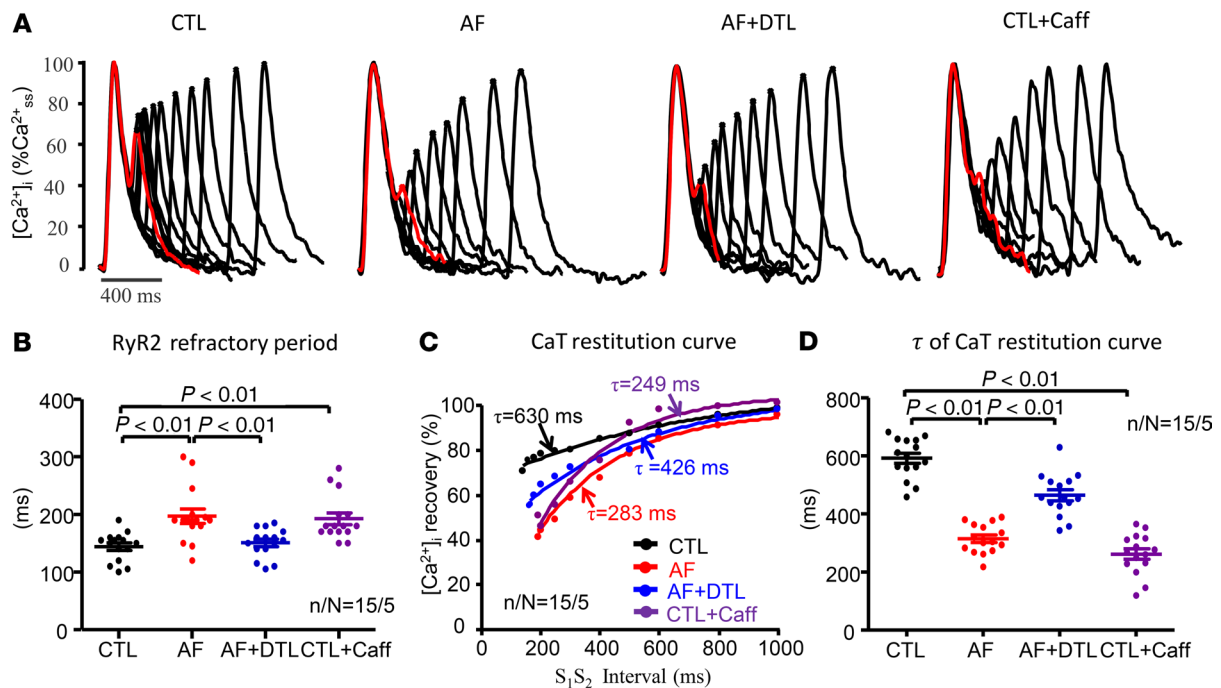
Figure 1. Original recordings of cardiomyocyte Ca²⁺ transients at different S1-S2 coupling intervals. (**A**) The basic Ca²⁺ transient (CaT) and the CaT at the shortest S1-S2 to respond (just beyond the refractory period) are shown in red. (**B**) Ryanodine receptor (RyR2) refractory period for each condition. Each point represents the result from 1 cell. Horizontal lines show mean ± SEM. n/N, cells/dogs per group. (**C**) Typical examples of Ca²⁺ release restitution curves under each condition. (**D**) Decay time constant (τ) of the Ca²⁺ release restitution curve under each condition. Each point represents the result from a single cell. Horizontal lines show mean ± SEM. n/N = 15 cells from 5 dogs per group for all measures (1-way ANOVA followed by Bonferroni's post hoc test).

We further quantified the spatial variability in Ca²⁺ release dynamics by comparing the restitution τs at multiple locations. Figure 5A shows representative CaT restitution curves at 4 atrial locations. The τs were smaller overall in AF atria than in CTLs (Figure 5B), corresponding to AF effects on single-ACM restitution (Figure 1C). In addition, AF substantially increased the spatial variability in restitution kinetics (Figure 5C).

Alterations in atrial CaT and action potential duration alternans in atrial tissues. We evaluated the effects of AF on ACM alternans in situ with simultaneous optical mapping of CaT and action potential duration (APD) alternans. Figure 6, A and B, illustrate, respectively, CaT and APD alternans thresholds in a CTL atrium. Recordings from single pixels are shown, along with maps at the left of the amplitude of beat-to-beat changes at each pixel in the recording field. Consistent with the single-ACM results, the median BCL thresholds for CaT and APD alternans were significantly increased in AF versus CTL atria (median CaT alternans threshold in CTL 200 ms vs. 255 ms for AF; APD threshold: 180 ms in CTL vs. 225 ms for AF, $P < 0.001$ for each; Figure 6, C and D). Of note, in all cases and conditions, Ca²⁺ alternans occurred at a longer cycle length threshold (by ~20 ms) than APD alternans (Supplemental Figure 4).

Effects of pharmacological modulation of cellular Ca²⁺ release behavior. To explore the relationship between RyR2 leakiness, increased CTR, and CaT alternans, we used dantrolene (10 μM) to suppress RyR2 leak (13). Dantrolene substantially reduced SCaS frequency, Ca²⁺ spark–mediated leak, and SCaT events in AF cardiomyocytes (Figure 3 and Supplemental Figure 3). The addition of dantrolene decreased CTR in ACMs from AF dogs toward CTL values (Figure 1, A and B: from 197 ± 13 ms in AF ACMs to 150 ± 6 ms in dantrolene-treated [AF + DTL] ACMs, $P < 0.01$). Dantrolene also moved the time course of CaT restitution in AF cells toward CTL values (Figure 1, C and D). Similarly, dantrolene increased the CaT alternans threshold in ACMs from AF dogs (Figure 2B), from a median of 3 Hz in AF to 4 Hz in AF + DTL ($P < 0.001$). Correspondingly, dantrolene decreased the BCL threshold for CaT and APD alternans in perfused atria from AF dogs (Figure 6, C and D). Dantrolene also returned the kinetic properties of AF-remodeled atrial Ca²⁺ restitution toward control values, increasing the S2/S1 CaT ratio (Figure 4B) and the τ of calcium release restitution (Figure 5B), while decreasing the COV ratio (Figure 4C) and COV τ (Figure 5C) in AF atria. Thus, reducing RyR2 leak with dantrolene reversed many of the abnormalities in CaT and APD kinetic properties associated with AF.
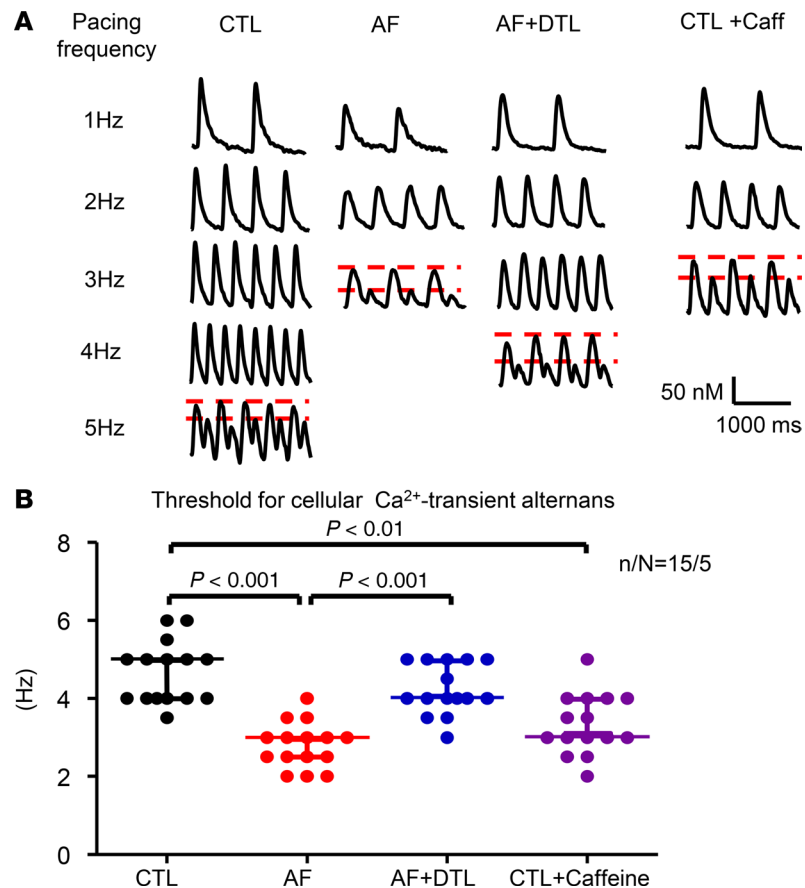
Figure 2. Cellular alternans in CaTs. (**A**) Examples of signals at progressively greater frequencies without and with alternans recorded, with results from 1 cell in each group shown in a column. (**B**) Threshold for cellular CaT alternans for each condition. Each point represents the result from a single cell. Horizontal lines show medians and interquartile range. n/N = 15 cells from 5 dogs per group for all measures. Nonparametric Kruskal-test. n/N, cells/dogs per group; CTL, control; AF, atrial fibrillation atrial cells; AF + DTL, dantrolene-treated AF cells; CTL + Caff, caffeine-treated CTL atrial cells.

To determine whether we could reproduce AF-associated abnormalities in isolated CTL dog cardiomyocytes by enhancing RyR2 leak, we applied low-dose caffeine (100 μM), known to increase RyR2 leak and SCaS frequency (14). Consistent with expectations, caffeine significantly increased SCaS frequency, Ca^{2+} spark–mediated leak, and SCaT events in CTL cardiomyocytes (Figure 3 and Supplemental Figure 3). The addition of caffeine increased CTR in ACMs from CTL dogs toward AF values (Figure 1, A and B: from 144 ± 7 ms in CTL cardiomyocytes to 193 ± 10 ms in caffeine-treated cardiomyocytes, $P < 0.01$). Caffeine also shifted the time course of $[Ca^{2+}]_i$ restitution toward AF values (Figure 1, C and D) and reproduced AF effects on cellular CaT alternans threshold (Figure 2). Correspondingly, caffeine increased the BCL threshold for CaT and APD alternans in perfused atria from CTL dogs (Figure 6, C and D). Caffeine also mimicked AF effects on restitution, decreasing the S2/S1 CaT ratio (Figure 4B) and τ of Ca^{2+} release restitution curves (Figure 5B), while increasing the COV ratio (Figure 4C) and COV τ (Figure 5C) in CTL atria.

Alternans behavior and AF. The results presented above show that AF-induced remodeling increases the susceptibility to CaT and APD alternans by altering CaT dynamics and increasing their heterogeneity. We then examined the relationship between alternans occurrence/pattern and AF induction. Representative recordings of the transition from spatially concordant alternans (SCA) to spatially discordant alternans (SDA) from an AF atrium are shown in Figure 7A. During dynamic pacing at threshold BCL, CaT and APD alternans were initially spatially concordant across the atrial surface. With further decreases in BCL, SCA transitioned to SDA. Whenever SDA CaT occurred, SDA APD alternans also appeared (Figure 7, B and C). The inducibility of SDA CaT/APD was significantly increased in AF atria (occurring in 6/8, or 75.0%, of AF atria vs. 0/6, or 0%, of CTL atria, $P < 0.01$); dantrolene reduced SDA CaT/APD incidence in AF atria from 75% to 1/8 (12.5%); caffeine increased SDA CaT/APD incidence in CTL atria from 0%
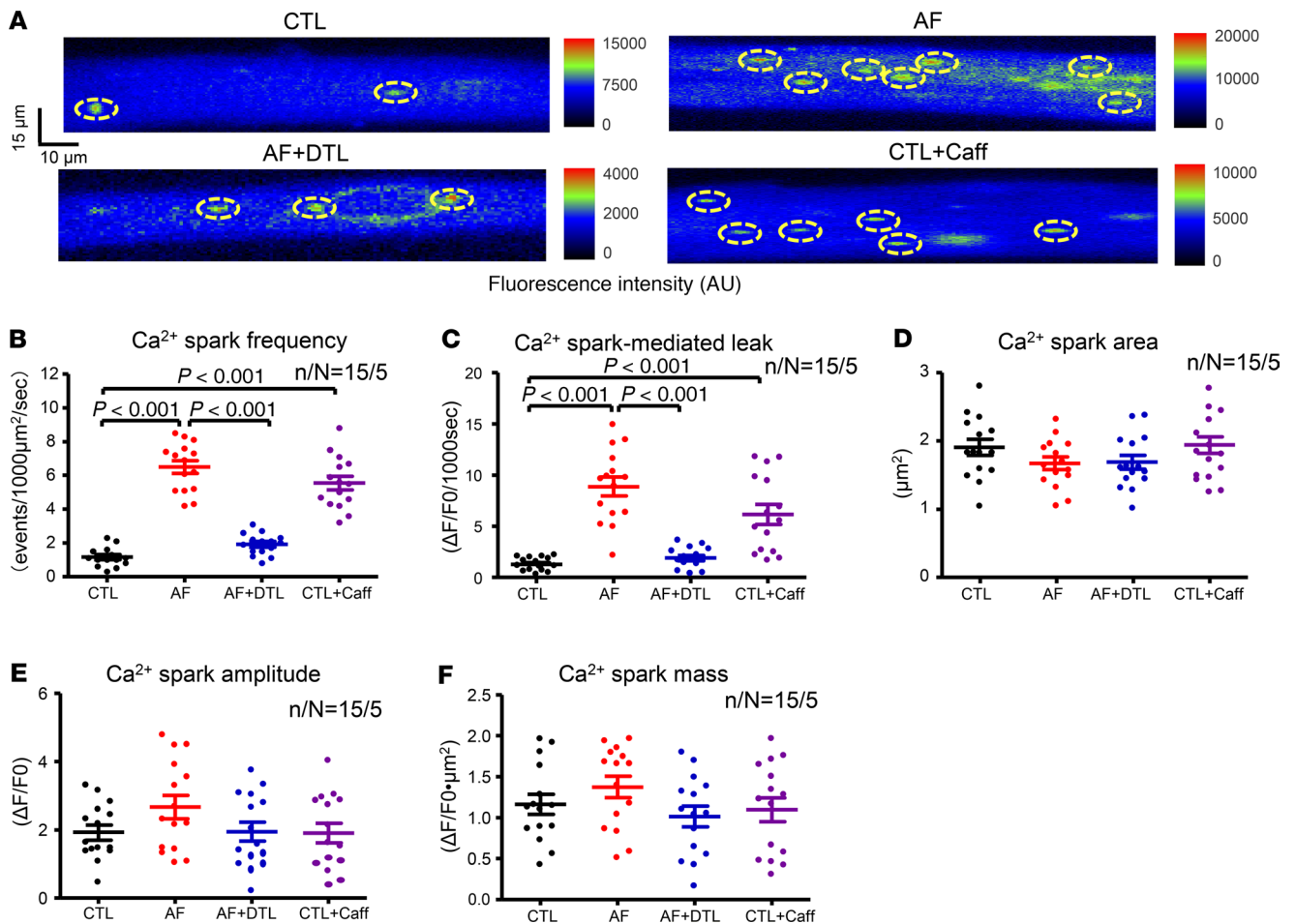
Figure 3. Cardiomyocyte spontaneous Ca²⁺ sparks on 2-dimensional confocal imaging. (A) Fluorescence imaging of $[Ca^{2+}]_i$ showing spontaneous Ca²⁺ sparks in each group. The yellow dashed ovals indicate sparks our analysis software identified for each condition. **(B–F)** Quantification of spontaneous Ca²⁺ spark frequency **(B)**, Ca²⁺ spark–mediated leak **(C)**, Ca²⁺ spark area **(D)**, Ca²⁺ spark amplitude **(E)**, and Ca²⁺ spark mass **(F)** under each condition. Each point represents the result from a single cell. Horizontal lines show mean ± SEM. n/N = 15 cells from 5 dogs per group for all measures. 1-way ANOVA followed by Bonferroni's post hoc test. AF + DTL, dantrolene-treated AF cells; CTL + Caff, caffeine-treated CTL atrial cells.

to 4/6 (66.7%, $P < 0.01$, Figure 7C). Upon the onset of SDA, the beat-to-beat behavior of discordant APD alternans paralleled that of Ca²⁺ alternans, with a somewhat smaller amplitude (Supplemental Figure 5).

The induction of AF was closely linked to that of SDA, appearing after the development of SDA in all cases and in none in which SDA failed to develop. AF was induced in 75% (6/8) of AF-remodeled atria, versus 0% of 6 CTL atria ($P < 0.01$). AF inducibility of AF atria was suppressed by dantrolene (to 1/8, 12.5%, of AF atria, $P < 0.01$); in contrast, AF inducibility of CTL atria was promoted by caffeine, occurring in 4/6, 66.7%, of CTL atria ($P < 0.05$). AF initiation was related to the development of functional block–associated reentry, as illustrated in Supplemental Figure 6. During discordant alternans associated with rapid pacing, the impulse blocked in a long APD region, inducing reentry around the line of block and reentrant rotor formation.

Figure 8 illustrates the relationship between zones of SDA and reentrant activity. Figure 8A shows a right atrial (RA) pseudo ECG from 1 optically mapped preparation. The ΔAPD map for complexes a and b (the penultimate paced complexes prior to AF initiation) are shown in the upper-left of Figure 8B. There are substantial and discordant interbeat APD differences between regions in the mapped area. The subsequent panels show phase maps corresponding to the time points indicated on the pseudo ECG. Dynamic pacing induced AF with consistent counterclockwise rotor activity in the field of view, as shown by the PSs at the core tip of the rotor at 8 snapshots of phase maps within a rotational cycle. The location of the core tip PS coincided closely with the location of nodal lines during SDA.

In vivo correlates. We then sought to determine whether the phenomena we studied at the cellular and isolated atrial level also occur in vivo. We recorded activation recovery intervals (ARIs) in anes-
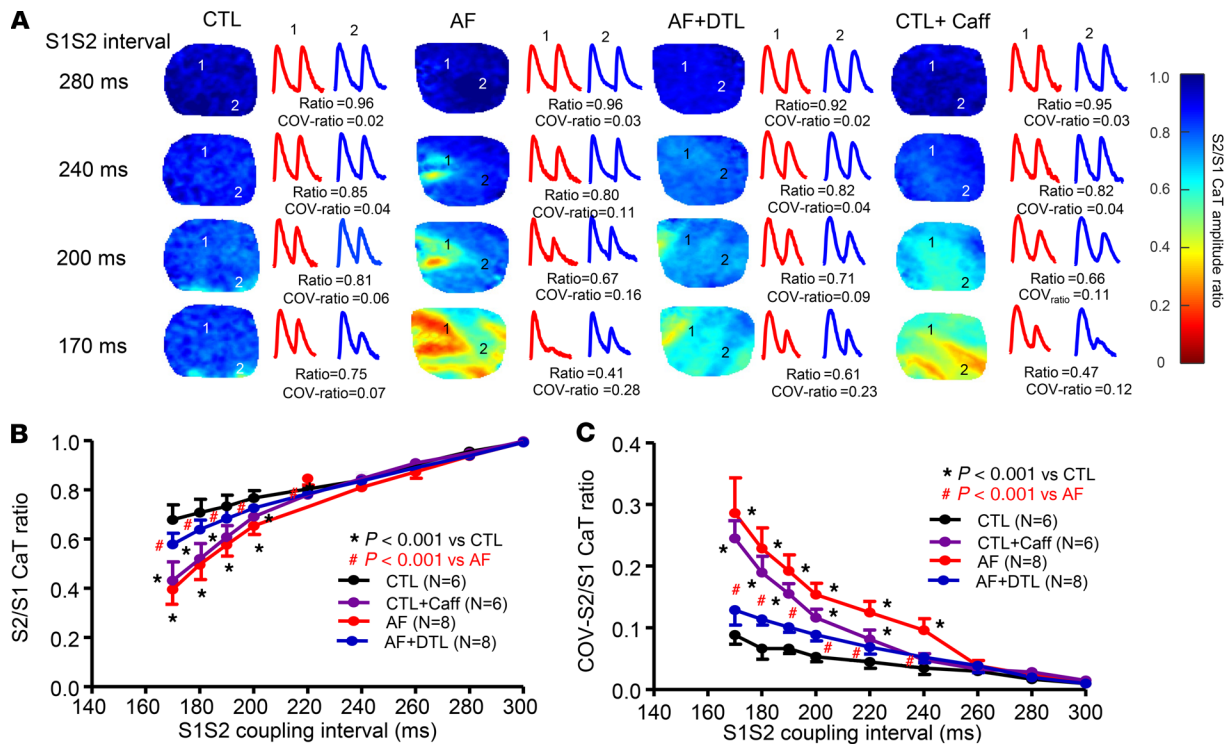
Figure 4. Spatial dispersion of CaT restitution properties upon optical mapping in situ. (A) Maps of S2/S1 CaT amplitude ratio (color scale at right) during progressive decreases in S1-S2 coupling interval for each condition (left columns). Original recordings of the basic CaT (the first CaT) and the premature stimulation–induced CaT (the second CaT) from sites 1 and 2 for each condition are shown in the right columns. **(B)** Average S2/S1 CaT amplitude ratio for different S1-S2 coupling intervals in each group. **(C)** Average coefficient of variation (COV) of S2/S1 (COV S2/S1) CaT amplitude ratio for different S1-S2 coupling intervals in each group. Horizontal lines show mean ± SD. $N = 6$ for CTL and CTL + Caff; $N = 8$ for AF and AF + DTL. 2-way repeated-measures ANOVA followed by Bonferroni-corrected post hoc tests. CTL + Caff, CTL atria after caffeine treatment; AF + DTL, AF atria after dantrolene treatment.

thetized CTL or AF dogs, before and after dantrolene (2.5 mg/kg, IV). Figure 9A shows representative recordings of atrial ARI alternans from a CTL dog, as well as in an AF dog, before and after dantrolene administration. Compared with CTL dogs, the median BCL threshold for ARI alternans was significantly increased in AF dogs (Figure 9B: AF 210 ms vs. CTL 150 ms, $P < 0.001$). Dantrolene administration significantly decreased the BCL threshold for ARI alternans in AF dogs (to 170 ms, $P < 0.01$). These results indicate that in vivo vulnerability to atrial APD alternans is increased in AF dogs and that dantrolene attenuated this effect.

Supplemental Figure 7 shows recordings of AF induction by atrial burst pacing in a CTL dog, along with an AF dog before and after dantrolene administration. Compared with CTL dogs, the AF vulnerability and AF duration were markedly increased in AF dogs (AF vulnerability: 61% ± 6% in AF vs. 5% ± 3% in CTL, $P < 0.001$; AF duration: 379 ± 96 s in AF vs. 14 ± 8 s in CTL, $P < 0.01$). Dantrolene administration markedly decreased the AF inducibility and AF duration in AF dogs (AF inducibility: 28% ± 7% in AF + DTL vs. 61% ± 6% in the same AF dogs before DTL; AF duration: 61 ± 23 s in AF + DTL vs. 379 ± 96 s in the same AF dogs before DTL; all $P < 0.01$).

Alterations in Ca²⁺ handling proteins. To gain insights into the potential molecular basis of abnormalities of Ca^{2+} handling in AF atria, we performed Western blots on a range of relevant proteins in isolated cardiomyocytes (for original images, see Supplemental Figure 8A; Supplemental Figure 9, A and B; and Supplemental Figure 10, A and B). AF significantly reduced the expression of total RyR2 (Supplemental Figure 8B), Ser2808-phosphorylated RyR2 (Supplemental Figure 8C), and the Ser2814-phosphorylated form (Supplemental Figure 8D). Phosphorylation ratios (Ser2808- and Ser2814-phosphorylated RyR2 to total RyR2) were not significantly affected (Supplemental Figure 8, E and F). Phospholamban (PLB) was not significantly affected by AF, including total PLB (Supplemental Figure 9C), the Ser16-phosphorylated form (Supplemental Figure 9D), and phosphorylation ratios (Ser16- and Thr17-phosphorylated PLB divided by total PLB; Supplemental Figure 9, F and G); nor was sarco/endoplasmic reticulum Ca²⁺-AT-
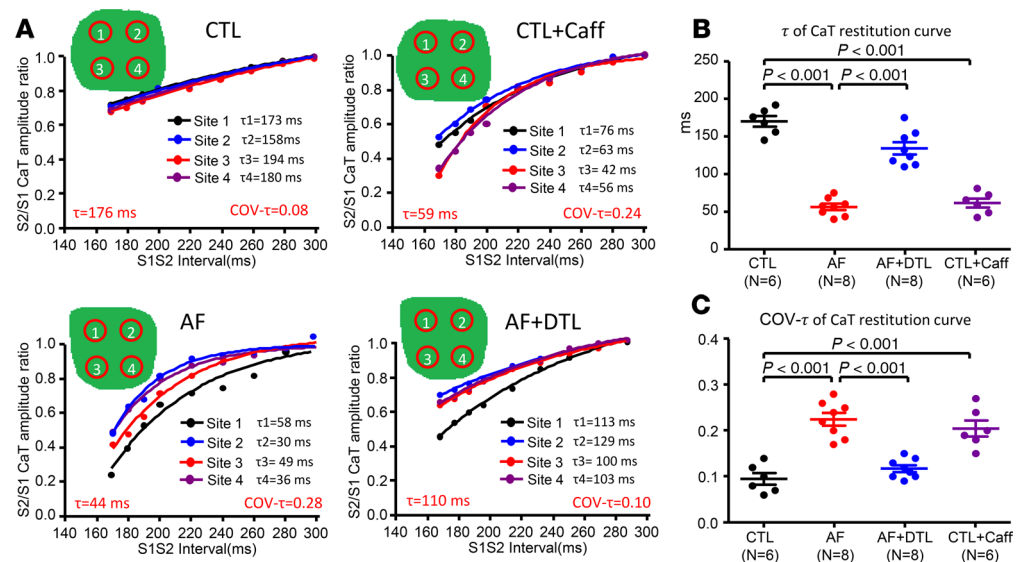
Figure 5. Changes in rate and spatial dispersion of Ca²⁺ release restitution upon optical mapping in situ. (**A**) Examples of CaT release restitution curves at 4 sites under each condition. The mean decay time constants (τ_ms) of 4 locations and the covariance are shown in red text under each panel. (**B**) Mean decay time constants (τs) of the CaT restitution curve under each condition (each point represents results from a single animal). (**C**) COV of τ of the CaT restitution curve under each condition. Horizontal lines show mean ± SEM. $N = 6$ for CTL and CTL + Caff; $N = 8$ for AF and AF + DTL. 1-way ANOVA followed by Bonferroni's post hoc test. CTL + Caff, CTL atria after caffeine treatment; AF + DTL, AF atria after dantrolene treatment; Cov, the covariance of the τ value, obtained by the ratio of SD divided by the mean value of τ.

Pase 2a (SERCA2a) (Supplemental Figure 9H). AF significantly increased the expression of Thr17-phosphorylated PLB ($P < 0.05$; Supplemental Figure 9E). FKBP12.6 expression was nonsignificantly reduced in AF (Supplemental Figure 10A), whereas calsequestrin (CSQ) showed a statistically significant, about 30%, decrease (Supplemental Figure 10B).

Discussion

In this study, we evaluated for the first time to our knowledge the relationships among Ca²⁺ mishandling induced by AF, the susceptibility to different forms of atrial alternans behavior in atrial tissues and intact hearts, and AF susceptibility. We relate findings in single cells to those in intact atria with the use of Ca²⁺ imaging and V_m analysis and to in vivo consequences with studies in intact, anesthetized dogs. Furthermore, the potential molecular changes underlying Ca²⁺ mishandling were studied with the use of immunoblots. Our results indicate that AF remodeling enhances spontaneous single-cell Ca²⁺ release, prolongs the refractory period of the CaT, increases the slope of the CaT restitution curve, and predisposes to CaT alternans. The AF-induced changes were mimicked in control cells by increasing spontaneous Ca²⁺ release with low-dose caffeine and suppressed in AF cells by dantrolene. Correspondingly, in coronary-perfused preparations, AF atria displayed increased Ca²⁺ handling heterogeneity and susceptibility to CaT and APD alternans, particularly SDA, which was associated with enhanced AF inducibility accompanied by rotor formation at nodal lines. Dantrolene decreased Ca²⁺ handling heterogeneity and suppressed alternans behavior and AF vulnerability in AF atria. Finally, in vivo studies in dogs with AF-induced remodeling confirmed increased susceptibility to rate-dependent atrial repolarization alternans, along with enhanced AF vulnerability and sustainability, which were attenuated by intravenous dantrolene administration.

Ca²⁺ handling changes in AF and potential arrhythmogenic role. A variety of Ca²⁺ handling abnormalities have been associated with AF, based on studies of both ACMs isolated from AF patients (6–9, 15) and experimental animals (16–18). Spontaneous diastolic Ca²⁺ release and RyR2 dysfunction are almost ubiquitous findings (6, 9, 16–19). Several studies show enhanced delayed afterdepolarizations resulting from diastolic Ca²⁺ leak, associated with spontaneous ectopic activation generation (8, 9, 16, 17, 19), although one report indicates Ca²⁺ silencing that protects against spontaneous Ca²⁺ release and activity (15).

Here, we confirmed an increase in spontaneous cellular Ca²⁺ release events in ACMs from AF dogs; moreover, this finding was associated with increased CTR, altered CaT restitution, and greater susceptibility
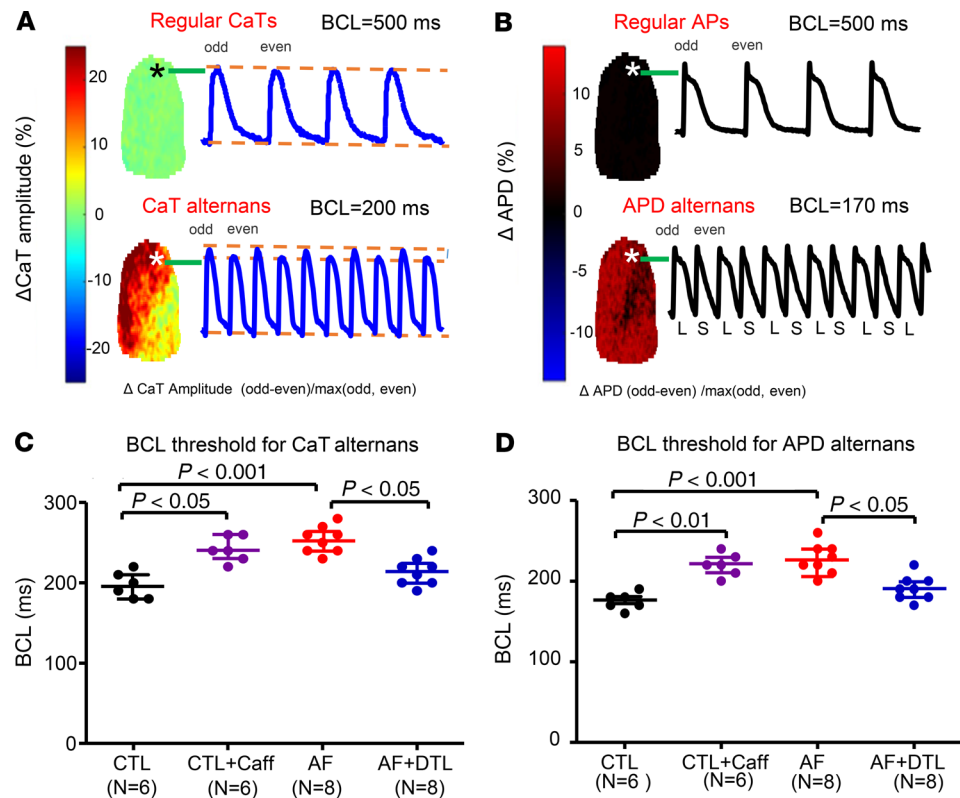
Figure 6. CaT and APD alternans thresholds in optically mapped preparations. (A) Example of CaT alternans from a CTL atrium. Top: ΔCaT amplitude map (left) and a CaT recording from a single pixel (position shown with star on map) at 500-ms basic cycle length (BCL). Bottom: ΔCaT amplitude map (left) and a CaT recording from a single pixel at 200-ms BCL. **(B)** Example of APD alternans from the same CTL atrium. Top: ΔAPD map (left) and action potential recording from a single pixel at 500-ms BCL. Bottom: ΔAPD map (left) and action potential recording at 170-ms BCL. BCL threshold for CaT **(C)** and APD **(D)** alternans in each group; each point represents the result from a single atrium. Horizontal lines show median values and interquartile range for BCLs that induced CaT or APD alternans. $N = 6$ for CTL and CTL + Caff; $N = 8$ for AF and AF + DTL. Nonparametric Kruskal-Wallis test. CTL + Caff, CTL atria after caffeine treatment; AF + DTL, AF atria after dantrolene.

to CaT alternans. A causative role of spontaneous Ca^{2+} leak in altered CaT kinetics was supported by the observation that low-dose caffeine reproduced the alterations AF caused and that dantrolene, which suppresses Ca^{2+} leak (13, 19), reversed the AF-induced changes. Further support for a role of Ca^{2+} mishandling in arrhythmogenesis was obtained by noting the relationship between CaT and APD alternans behavior in AF dog atria, which caused SDA and associated rotor formation along with greatly increased AF susceptibility. Again, these changes were suppressed by dantrolene. Finally, we obtained evidence for similar phenomena in vivo. These results argue strongly that Ca^{2+} mishandling due to AF remodeling plays a role in AF promotion not only by favoring ectopic impulse formation but also by increasing the susceptibility to reentry.

Alternans behavior in clinical AF. A wide range of observations point to the importance of repolarization alternans in clinical AF (20). Since the first report of atrial monophasic APD alternans in a patient with atrial tachycardia (21), a number of studies have confirmed the occurrence and potential pathophysiological role of alternans in AF. Kim et al. showed increased APD restitution slope in patients with AF versus controls (22). Narayan et al. demonstrated that APD alternans occurred at much lower rates in patients with AF than controls and disorganized to complex oscillations leading to AF as rate increased further (23). In the latter 2 studies, altered repolarization kinetics occurred in patients with both persistent AF and paroxysmal AF. Patients with persistent AF were cardioverted just before electrophysiological study and were therefore quite analogous to our AF dogs, which had electrically maintained AF until the terminal experiment. Although patients with paroxysmal AF do not have AF-induced remodeling per se, they show spontaneous cellular Ca^{2+} release (9), which our findings suggest might explain their susceptibility to APD alternans.

Recent computational modeling studies further support the role of Ca^{2+} handling abnormalities in atrial alternans and clinical AF. Chang et al. used a human atrial tissue model incorporating AF-associated
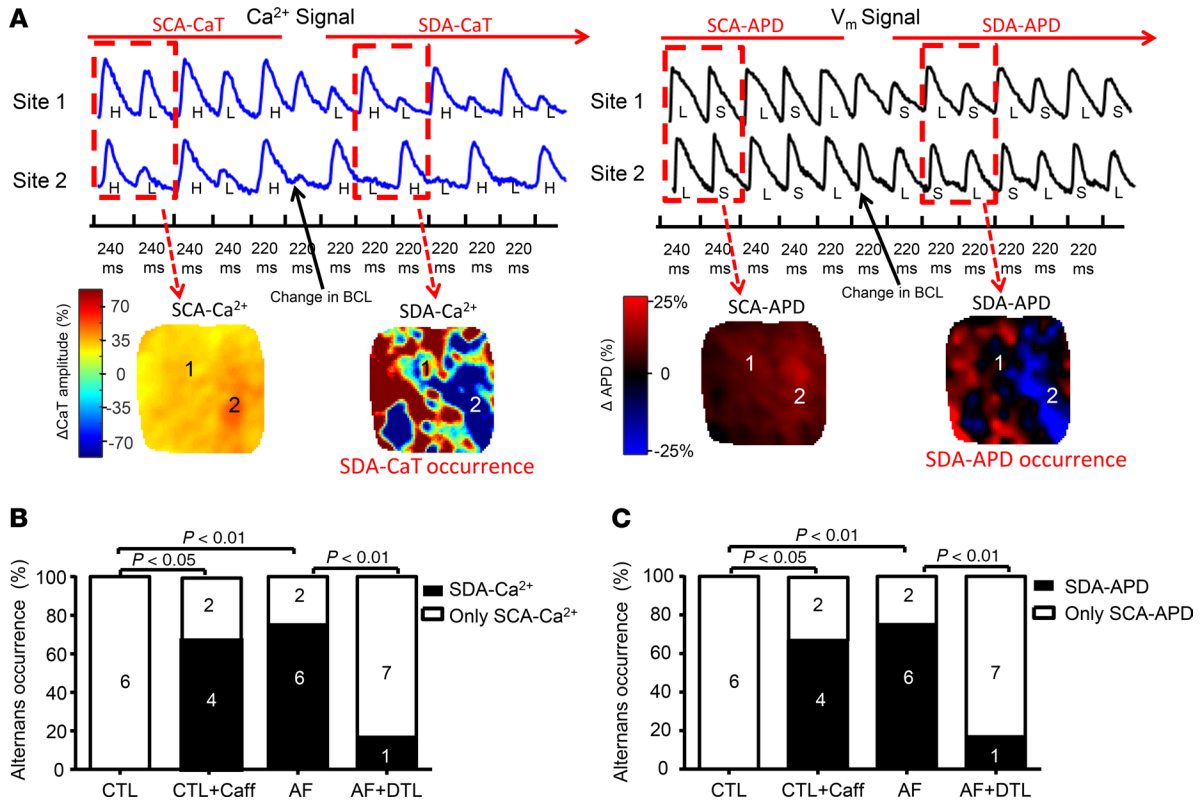
Figure 7. Relationship between SDA of CaT and SDA APD. (A) Representative recordings of the transition from SCA to SDA in CaT and APD from a single AF atrium upon reducing BCL from 240 ms to 220 ms. SDA CaT and SDA APD occurred simultaneously. Top: CaT and corresponding action potential recordings at the same 2 sites. Bottom: ΔCaT amplitude map and corresponding ΔAPD map; positive and negative APD alternans phases are represented by red and blue, respectively. **(B** and **C)** Inducibility of SDA CaT **(B)** and SDA APD **(C)** in each group. The vulnerability to SDA Ca^{2+} and SDA APD was significantly increased in AF atria; DTL suppressed SDA Ca^{2+} and SDA APD in AF atria. $N = 6$ for CTL and CTL + Caff; $N = 8$ for AF and AF + DTL. χ^2 test. CTL + Caff, CTL atria after caffeine treatment; AF + DTL, AF atria after dantrolene.

electrophysiological remodeling and performed a sensitivity analysis of ion channel/transporter properties that might be involved in alternans behavior (11). They concluded that decreased RyR2 inactivation is the only parameter variation that reproduces AF-associated APD alternans behavior at relatively slow rates and that RyR2 kinetics may play a critical role in governing proarrhythmic APD alternans. In a subsequent study with a 3-dimensional human atrial model, they noted a critical role of Ca^{2+}-driven alternans, not only in the initiation of AF, but also in its persistence by causing unstable scroll waves that meander and break up to produce multiple daughter wavelets (24).

Spatially concordant and discordant alternans. Alternans can be spatially concordant or discordant (25, 26). SCA occurs when all the cells are alternating in phase, can be induced by rapid pacing in most normal hearts, and is not necessarily arrhythmogenic. By contrast, SDA is more malignant and frequently observed in pathological states. The large refractory gradients over short distances resulting from SDA can produce conduction block and reentrant excitation that results in tachyarrhythmias and fibrillation (25–27). In our optical mapping study, SCA was induced in all atria, both CTL and AF, but SDA occurred in 0% of CTL atria versus 75% of AF atria. Furthermore, SDA immediately preceded AF onset in all 6/6 AF atria.

To gain insights into the much greater susceptibility of AF atria to SDA CaT, we studied the spatial heterogeneity of Ca^{2+} handling. We found a clear increase in Ca^{2+} handling heterogeneity in AF atria, evidenced by increased COV S1/S2 ratios and COV τ of the Ca^{2+} release restitution curve. The increased Ca^{2+} handling heterogeneity was associated with a transformation from SCA CaT to SDA CaT upon abrupt BCL reduction in AF atria. Dantrolene decreased Ca^{2+} handling heterogeneity and abrogated SDA Ca^{2+} occurrence in AF atria. By contrast, low-dose caffeine increased Ca^{2+} handling heterogeneity and increased the inducibility of SDA CaT in CTL atria. These findings implicate spatial heterogeneity in Ca^{2+} handling remodeling in the occurrence of SDA CaT.
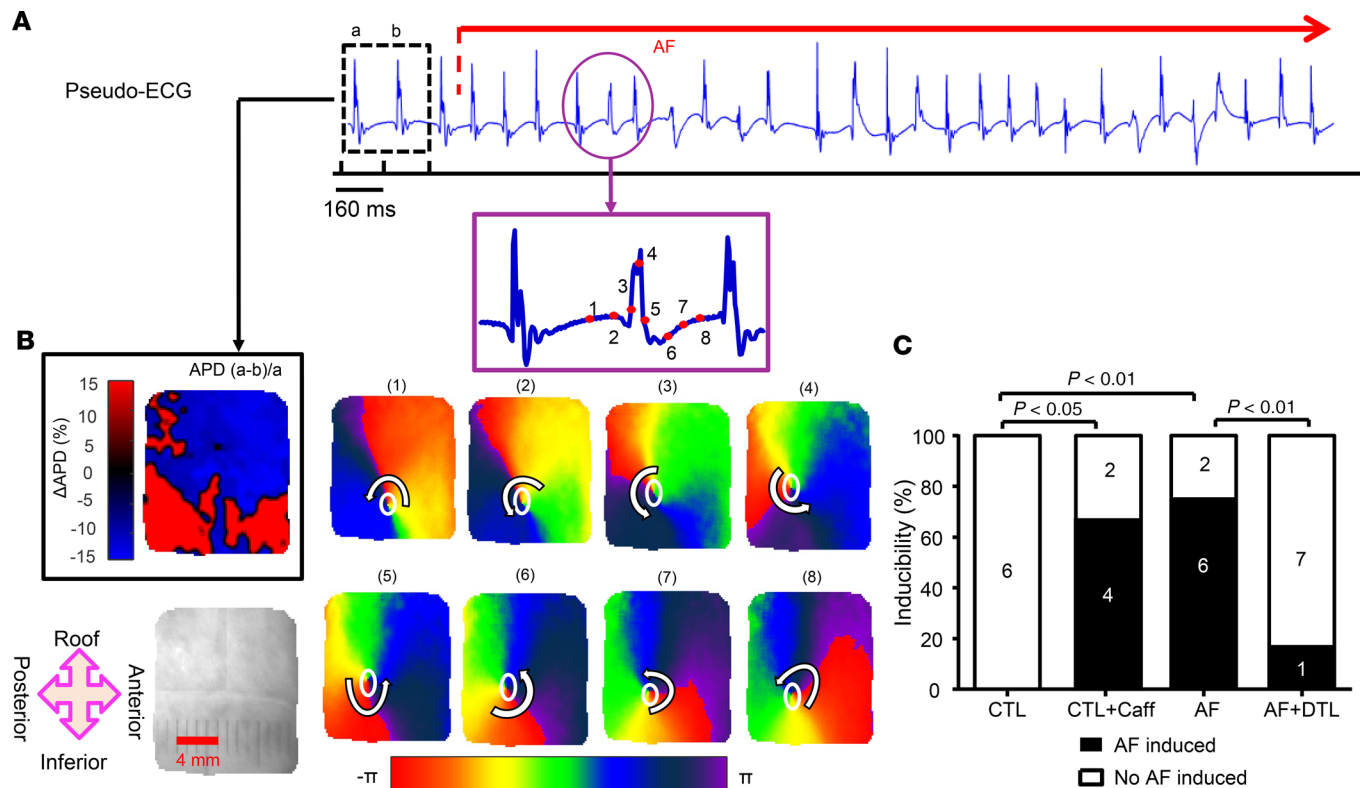
Figure 8. Initiation of AF in 1 optically mapped AF atrium. (A) Right atrium pseudo ECG during AF initiated by pacing at 160-ms BCL. (**B**) Upper-left panel shows the ΔAPD map for complexes corresponding to cycles a and b on the pseudo ECG (the penultimate paced complexes prior to AF initiation). The subsequent panels show 8 snapshots of phase maps corresponding to the time points indicated in red points of the amplified pseudo ECG episode. The positions of phase singularities (PSs) are indicated by white ovals. (**C**) Inducibility of AF in each group. The vulnerability to AF was significantly increased in AF atria; DTL reduced AF vulnerability in AF atria, whereas Caff enhanced AF vulnerability in CTL atria. $N = 6$ for CTL and CTL + Caff; $N = 8$ for AF and AF + DTL. χ² test. CTL + Caff, CTL atria after caffeine treatment; AF + DTL = AF atria after dantrolene treatment.

The mechanism for SDA APD is still poorly understood. In this study, we observed that SDA CaT and SDA APD always occurred concurrently in atrial tissue. Dantrolene and low-dose caffeine administration, which affected the occurrence of SDA CaT, abrogated and promoted the occurrence of SDA APD, respectively. These results suggest that SDA CaT is central to the development of SDA APD.

Potential mechanisms underlying Ca²⁺ handling abnormalities. Cellular Ca²⁺ handling is a complex process involving a wide range of proteins involved in Ca²⁺ transport, subcellular organelles and architecture, and regulatory processes. A number of molecular mechanisms have been implicated in CaT alternans. SERCA2a is responsible for cytosolic Ca²⁺ uptake. SERCA2a downregulation is a classical feature of cellular remodeling in heart failure, conspiring with increased RyR2 leak and PLB hypophosporylation to reduce ventricular cardiomyocyte Ca²⁺ stores and cause hypocontractility (28). SERCA2a downregulation is a principal correlate of repolarization alternans in heart failure (29), and alternans and arrhythmogenesis are suppressed by SERCA2a gene transfer (30). However, SERCA2a expression was not changed in our AF ACMs (Supplemental Figure 9H). Consistent with our observation, SERCA2a overexpression and inhibition had little effect on alternans behavior in rat ACMs (31). Similarly, enhancing SERCA2a function with a gain-of-function PLB mutation or mildly suppressing SERCA2a function had minimal effects on Ca²⁺ alternans in mouse hearts (32).

A number of recent studies suggest that enhanced RyR2 Ca²⁺ leak can cause cellular CaT alternans (10, 33). Local Ca²⁺ sparks promote CaT alternans by a spark-induced spark mechanism in a computational model (34). Post–myocardial infarction dogs with enhanced RyR2 leak due to redox modulation of RyR2 similarly show susceptibility to CaT alternans (35). These observations are consistent with our findings indicating a central role of AF-induced RyR2 Ca²⁺ leak in CaT and APD alternans. Mathematical modeling of the complex determinants of Ca²⁺ alternans does predict, at least under certain conditions, increased Ca²⁺ spark rate increasing the likelihood of alternans (33). On the other hand, extensive observations suggest that, on the contrary, enhancing RyR2 function (e.g., with caffeine) reduces RyR2 refrac-
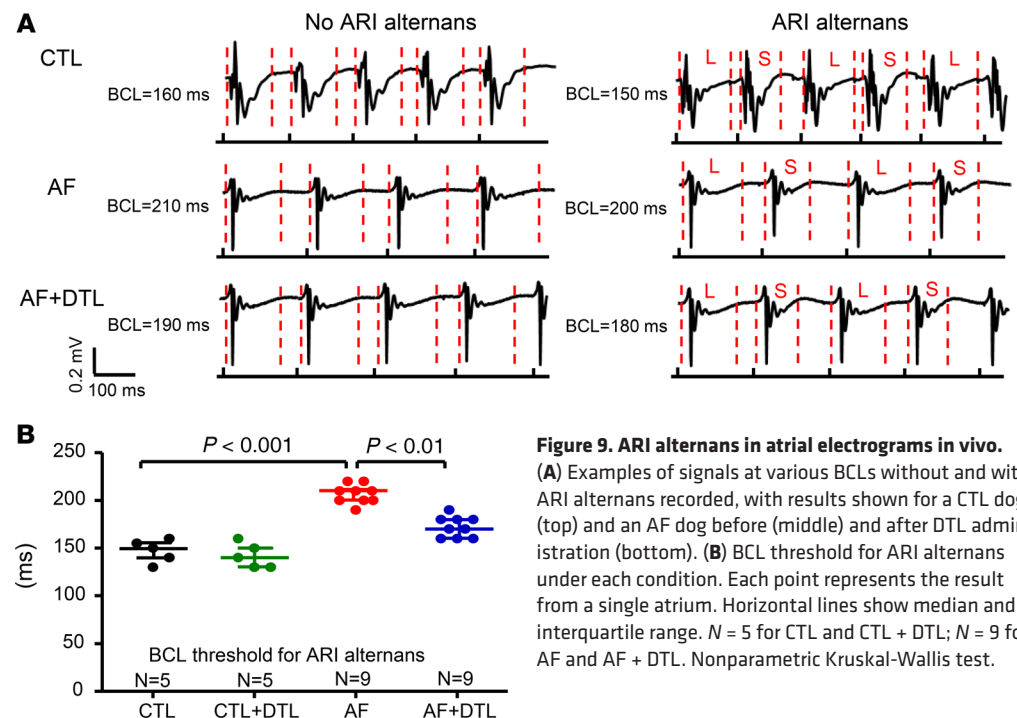
Figure 9. ARI alternans in atrial electrograms in vivo. (**A**) Examples of signals at various BCLs without and with ARI alternans recorded, with results shown for a CTL dog (top) and an AF dog before (middle) and after DTL administration (bottom). (**B**) BCL threshold for ARI alternans under each condition. Each point represents the result from a single atrium. Horizontal lines show median and interquartile range. N = 5 for CTL and CTL + DTL; N = 9 for AF and AF + DTL. Nonparametric Kruskal-Wallis test.

toriness (thereby alleviating Ca^{2+} alternans) whereas suppressing RyR2 Ca^{2+} release promotes alternans. For example, Sun et al. found that a gain-of-function RyR2 mutation shortened Ca^{2+} release refractoriness and suppressed alternans in the mouse ventricle (32). Interestingly, the mutation did not cause spontaneous Ca^{2+} release events, unlike the effect of AF in our model. Similarly, Wang et al. noted that sensitizing RyR2 with 200 μM caffeine suppressed alternans in the ventricles of isolated rabbit hearts (5). Alternans is clearly a complex and multifactorial phenomenon, but the refractoriness of the cellular Ca^{2+} transient is clearly a key determinant of atrial Ca^{2+} alternans (36), as we observed in the present study.

SR Ca^{2+} overload is well recognized to promote diastolic Ca^{2+} leak in cardiomyocytes (16). We observed increased SR Ca^{2+} content in AF-remodeled atria, likely resulting from 2 primary mechanisms: (a) increased SERCA2a-mediated SR Ca^{2+} uptake due to reduced PLB inhibition of SERCA2a caused by PLB hyperphosphorylation via CaMKII (Thr17 PLB) and (b) decreased SR Ca^{2+} release caused by down-regulated RyR2 expression (16, 37).

In addition to the increased SR Ca^{2+} loading, we found a significant reduction in CSQ expression in AF-remodeled atria. CSQ is the major Ca^{2+} binding protein in the SR and acts as a Ca^{2+} buffer regulating SR free Ca^{2+} concentration (38). CSQ may also inhibit RyR2 Ca^{2+} release independently of its buffering action. In heterozygous CSQ-knockout mice, moderate reductions (about 25%) in CSQ expression can increase SR Ca^{2+} leak and arrhythmia susceptibility in the presence of β-adrenoceptor stimulation (39). In CSQ-knockout mice, spontaneous atrial Ca^{2+} sparks are increased, and atrial tachypacing induces AF/flutter, which can be suppressed by the RyR2 inhibitor (R)-propafenone (40). These findings suggest that the reduced CSQ expression that we noted in AF ACMs (Supplemental Figure 10) may at least in part explain the spontaneous RyR2 leak that we observed. Finally, we found a reduction in RyR2 expression in AF ACMs (Supplemental Figure 8). Genetic suppression of RyR2 function prolongs Ca^{2+} release refractoriness and promotes Ca^{2+} release alternans in mouse hearts (41), suggesting that the RyR2 downregulation that we observed may also have contributed to the cellular phenotype.

Potential limitations. In this study, we noted that increased SR Ca^{2+} leak as quantified by spontaneous Ca^{2+} spark activity was associated with and paralleled prolonged CTR, which in turn was closely associated with Ca^{2+} and APD alternans. The refractory period of the CaT has multiple determinants, including L-type Ca^{2+} current (I_{CaL}) properties, SR Ca^{2+} load, and the intrinsic refractoriness of RyR2. I_{CaL} is known to be reduced in AF (42), and this change could have contributed to the alterations in CTR that we noted. In addition, caffeine and dantrolene would both be expected to alter SR Ca^{2+} stores, which could also affect CTR. Changes in diffusional distance between RyR2 clusters in association with changes in cellular ultrastructure and alterations

in intracellular buffering could also have played a role. Much more detailed studies of beat-to-beat changes in the relationships among SR Ca^{2+} stores, I_{CaL}, and SR Ca^{2+} release will be needed to determine the precise mechanisms underlying the changes in CTR that we observed with AF, caffeine, and dantrolene.

We used a single animal model for this study, electrically maintained AF for 1 week in the dog. We used this model to test a specific hypothesis: that AF-induced Ca^{2+} handling remodeling can affect the recovery of the CaT and thereby affect alternans behavior and the susceptibility to reentry. However, we cannot know whether different durations of AF might have different effects. Furthermore, many animal models are available for the study of AF (43), and there is no a priori reason to think that similar changes occur in other models. In addition, the model does not consider the effects of structural modeling, such as atrial fibrosis, which plays a key role in AF pathophysiology (1, 44).

In the dual optical mapping studies, the probes for $[Ca^{2+}]_i$ and V_m imaging share the same excitation band but have distinct emission bands. The fluorescence signals Rhod-2, AM, and RH 237 dyes emitted showed a shallow band of crosstalk in the emission spectra. Fluorescence signals were separated into different detectors using dichroic mirrors and emission filters. The 2 charge-coupled device (CCD) cameras must be precisely aligned to ensure that CaT and V_m signals are indeed acquired from the same myocardial sites. We aligned the cameras with a grid reference placed in the field of view, and absolute precision of alignment cannot be ensured.

Novel findings and significance. The principal potentially novel finding of this study is that AF-associated Ca^{2+} handling abnormalities predispose not only to spontaneous atrial ectopic firing, as previously noted (8, 9), but also to the initiation and maintenance of atrial reentry. This observation places Ca^{2+} handling disturbances squarely in the center of AF-promoting mechanisms and supports efforts to design novel compounds that improve Ca^{2+} handling to suppress AF (2, 45, 46).

There have been prior studies that demonstrate beneficial effects of dantrolene on cellular abnormalities in AF models. Avula et al. (19) showed that sheep with myocardial infarction have spontaneous Ca^{2+} release–related atrial ectopic activity that initiates atrial reentry and that dantrolene can suppress both ectopic firing and spontaneous AF episodes in the sheep. Their study followed up on prior work demonstrating Ca^{2+}-driven atrial ectopy in a canine model of chronic atrial infarction (17). Hartmann et al. (47) similarly showed that dantrolene suppresses Ca^{2+} sparks and delayed afterdepolarizations in ACMs from patients with AF. Our work differs from these studies in assessing the relationships between AF-induced changes in Ca^{2+} handling, cellular alternans behavior, and reentry susceptibility, along with assessing in detail dantrolene's effects on the substrate for reentry rather than just the trigger, subjects that have not been addressed before in the literature, to our knowledge.

Our study potentially explains a consistent observation that has been somewhat enigmatic. In mouse models with aberrant Ca^{2+} handling and spontaneous Ca^{2+} releases, AF inducibility and persistence are consistently increased (18, 40, 48, 49). Furthermore, suppression of abnormal Ca^{2+} releases reduces susceptibility to AF induction and the persistence of any AF induced. Arrhythmia inducibility and maintenance are generally related to the reentrant substrate, and it has been unclear why they should be altered by spontaneous Ca^{2+} leak events. Our observation that spontaneous Ca^{2+} release leads to repolarization alternans that facilitates reentrant AF induction and maintenance can potentially explain the prior findings. Furthermore, the observation that a clinically available agent, dantrolene, suppresses the induction of SDA CaT and SDA APD in association with reduced AF vulnerability and AF sustainability points to the potential translational relevance of our findings to the search for new antiarrhythmic drug targets and agents for the treatment of this very common and problematic condition.

Methods

Canine AF model. Adult male mongrel dogs (20 to 35 kg) were obtained from LAKA Inc (9319.2763) and assigned to CTL and AF groups. After ketamine (5.3 mg/kg, IV)/diazepam (0.25 mg/kg, IV)/1.5% isoflurane anesthesia, AF dogs underwent fluoroscopically guided bipolar pacing lead insertion into the RA appendage and connection to a pacemaker in the neck. After 24 hours' postoperative recovery, dogs were atrial paced at 600 bpm to maintain fibrillatory atrial activity for 7 days. The CTL animals were handled identically to AF dogs, but their pacemaker was not activated.

Cardiomyocyte isolation. ACMs were isolated from the left atrium (LA) as described previously (16). Dogs were anesthetized with intravenous morphine (2 mg/kg) and alpha-chloralose (120 mg/kg). After intra-atrial injection of heparin (10,000 U), the heart was quickly removed and placed in Tyrode's solution containing (mM): NaCl 136, KCl 5.4, $MgCl_2$ 1, $CaCl_2$ 2, NaH_2PO_4 0.33, HEPES 5, and dextrose 10 (pH 7.35; NaOH).

The left coronary artery was cannulated, and the LA tissue was dissected free and perfused with 1.8 mM Ca^{2+} containing Tyrode's solution (37°C, 100% O_2). Leaks from arterial branches were ligated, and tissues were perfused with Ca^{2+}-free Tyrode's solution for 15 to 20 minutes, followed by Ca^{2+}-free Tyrode's solution containing collagenase (~0.45 mg/mL, CLS II, Worthington) plus 0.1% bovine serum albumin (MilliporeSigma) for 1 hour. Digested tissue was carefully minced and agitated, and LA ACMs were harvested. After isolation, cells were kept in 0.2 mM Ca^{2+}-containing Tyrode's solution for Ca^{2+} imaging experiments (16).

Ca^{2+} microfluorometry. ACMs were incubated with Indo-1 AM (5 μM) in 100 μM Pluronic F-127 (both from Invitrogen) and 0.05% dimethyl sulfoxide for 15 to 20 minutes, then superfused with normal Tyrode's solution (1.8 mM Ca^{2+}) for 20 minutes to allow intracellular de-esterification. Ultraviolet light passing through a 340-nm interference filter (Ionoptix LLC) was applied for excitation. Emitted light was detected by matched photomultiplier tubes. The fluorescence signal ratios ($R_{400/500}$) were digitized and converted to $[Ca^{2+}]_i$ with the formula $[Ca^{2+}]_i = Kd \times \beta \times (R_{400/500} - R_{min})/(R_{max} - R_{400/500})$ (50).

CTR was determined with an S1S2 protocol (51). CaTs were induced with field stimulation at 1 Hz for 10 seconds (S1), followed by a single S2 pulse. A series of S1S2 pulse protocols with progressively decreased S1-S2 coupling intervals (from 1000 to 100 ms) was applied while CaTs were continuously recorded. CTR was defined as the longest S1-S2 coupling intervals that failed to induce a CaT. The Ca^{2+} release restitution curves were constructed by plotting each S2/S1 CaT ratio against the corresponding S1-S2 coupling interval. The resulting data points were fitted with a single exponential function.

Caffeine-induced CaTs and corresponding NCX currents were simultaneously recorded in ACMs for quantification of SR Ca^{2+} content. Membrane potential was held at 80 mV. SR Ca^{2+} content was assessed by rapidly applying caffeine (10 mmol/L) after 1 minute of Ca^{2+} loading with continuous pacing. Caffeine-induced NCX current was integrated to calculate SR Ca^{2+} content (8).

Confocal Ca^{2+} imaging. To assess SCaSs, ACMs were incubated with 10 μM Fluo-4 AM (Invitrogen, Thermo Fisher Scientific) for 15 minutes. Subsequently, ACMs were placed on glass coverslips and superfused with 1.8 mM Ca^{2+}-containing Tyrode's solution for 10 minutes to allow intracellular de-esterification. Fluorescence images (16 bits, 10-ms intervals, pixel size = 0.2 μm) were acquired with a ZEISS LSM 5 LIVE confocal fluorescence microscope equipped with a 63×/1.4 Plan Apochromat oil objective. Fluo-4 AM was excited with a 488-nm argon laser, and emission signals were collected over 505 nm. Background subtracted fluorescence emission signals (F) were normalized to baseline fluorescence (F_0) by averaging 20 images. The changes in $[Ca^{2+}]_i$ are presented as $\Delta F/F_0$ (where $\Delta F = F - F_0$) (52). The SCaS frequency was calculated according to previously described approaches (53). Briefly, a region mask was chosen to define the cell outline and prevent interference from the cell exterior. A nonlinear partial differential equation–based method was combined with anisotropic diffusion and median filtering to improve signal-to-noise ratio. Fourth-order diffusion was applied to smooth small gradient noisy areas, while the areas having larger gradients remained nondiffused (54). Median filtering was applied subsequently to remove impulsive spikes generated by noise (55). The detection step used image segmentation to determine spark regions. Morphology dilation was performed first, and then connected components were labeled, followed by calculation of spark numbers and size. After finishing the preliminary calculation of sparks for each frame, the spark number was verified and counted. For spark centers that were in the region of a prior spark, the newly detected sparks were considered a continuation of the event in the previous frame and assigned the same ID number. The variables analyzed included Ca^{2+} spark frequency, spark area, spark amplitude, spark mass, and spark-mediated leak. The spark frequency was calculated as the total detected Ca^{2+} events over the recording time in the cell area of field of view. Spark amplitude was measured by the ratio of maximum F/F_0 at a spark event, indicating the highest relative fluorescence ratio. The spark area was measured at the time of maximum spark amplitude. The spark mass was calculated as spark amplitude × spark area × 0.33(change in fluorescence/initial fluorescence [$\Delta F/F_0 \times \mu m^2$]) and SR Ca^{2+} spark mediated–leak = spark mass × spark frequency($\Delta F/F_0 \times S^{-1}$), using a similar method to Benoist et al.'s method of Ca^{2+} spark detection (56).

Optical mapping of V_m and $[Ca^{2+}]_i$. The right atrium was dissected free, and the right coronary artery was cannulated and perfused with Krebs solution (in mM: 120 NaCl, 4 KCl, 1.2 $MgSO_4$ 0.7, 1.2 KH_2PO_4, 25 $NaHCO_3$, 5.5 glucose, 1.25 $CaCl_2$; in 95% O_2/5% CO_2) at 20 mL/min and 37°C. Any leak from arterial branches was ligated with silk thread to maintain adequate perfusion. After 10 minutes of stabilization and electromechanical uncoupling with blebbistatin (15 μM) (57), the preparation was loaded with Rhod-2, AM (Invitrogen, Thermo Fisher Scientific), and RH 237 (MilliporeSigma) for simultaneous optical mapping of CaT and V_m. Subsequently, the tissue was excited with a laser (Thorlabs) at a wavelength of 520 ± 45 nm. The bandpass filters for RH 237 and Rhod-2, AM, were 675 ± 25 nm and 590 ± 15 nm, respectively

(58, 59). Fluorescence images were recorded with 2 CCD cameras (CardioCCD, Redshirt Imaging) focused on a 1.5×1.5 cm^2 region. A pair of bipolar electrodes were positioned on the superior RA appendage, and the pacing stimuli were 2 ms pulse widths $\times$ 1.5′threshold square wave current.

Ca^{2+}/APD alternans was elicited during S1-S1 pacing with 15-second pulse trains separated by 30-second intervals to minimize pacing memory. Starting at 500 ms, the BCL was shortened to 300 ms in 100-ms intervals, to 180 ms in 20-ms intervals, and then in 10-ms steps until Ca^{2+}/APD alternans was induced. APD$_{80}$ was calculated as the time from maximal upstroke velocity (dF/dt$_{max}$) to 80% repolarization. CaT or APD alternans was quantified by subtracting the CaT amplitude or APD$_{80}$ for consecutive beats; alternans was defined as interbeat CaT amplitude or APD$_{80}$ differences averaging more than 5% over 6 stimuli. The threshold BCL was defined as the maximum BCL that induced Ca^{2+} or APD alternans.

To assess the transition from spatial concordant to discordant Ca^{2+}/APD alternans, the BCL was decreased from the APD alternans threshold BCL in 10-ms steps until AF was induced or 1:1 capture failed. AF was defined as a rapid (>400 bpm) irregular atrial rhythm lasting more than 1 second. If AF lasted more than 30 seconds, a 5-minute rest period was allowed after AF termination. The phase of alternans was termed positive for long short APD sequences (or high low CaT sequences), and negative for short long APD sequences (or low high CaT sequences). To evaluate spatial characteristics, alternans was classified as SCA or SDA. SCA was defined by at least 10% of the field of view displaying alternans that was entirely in phase. SDA was defined when the field of view simultaneously displayed both positive- and negative-phase alternans, with both positive and negative alternans occupying more than 10% of the surface area.

CTR was determined with an S1-S2 protocol (51). A single extrastimulus (S2) was delivered after 10 consecutive S1 stimuli at a BCL of 300 ms and decremented in 10-ms steps until failure to elicit a CaT. To quantify CaT recovery from refractoriness, we evaluated the ratio of the S2-induced CaT amplitude to the S1-induced CaT amplitude (S2/S1 CaT ratio) at S1-S2 coupling intervals ranging from 300 to 170 ms for each condition (5). Maps of S2/S1 CaT ratio were constructed at different S1-S2 coupling intervals for each condition. The Ca^{2+} release restitution curves were constructed by plotting the S2/S1 CaT ratio against the corresponding S1-S2 coupling interval. The resulting data points were fitted with a single exponential function. The Ca^{2+} release restitution curves were constructed in 4 locations. The decay τ of each Ca^{2+} release restitution curve was determined to calculate the average τ of the restitution curve. The COV (SD/mean) of the S2/S1 CaT ratio (COV ratio) and of the Ca^{2+} release restitution τ (COV τ) was determined to evaluate the spatial dispersion of Ca^{2+} handling.

Phase analysis was used to detect and follow PSs (60, 61). Hilbert transformation was performed first on the filtered signal from each pixel with the mean value during the recording period. The phase angle (θ) was calculated as the inverse tangent of the imaginary versus real part of the transformation result. Singularity detection was performed by using the concept of topological charge, implemented as a series of convolution operations. PSs were identified by a topological charge of ± 1 (62). The algorithm was implemented as a line integral of differential phase maps around each pixel on an 8-pixel length enclosed path. The pixels around which the phase progresses through a complete cycle from $-\pi$ to π are of great interest (63). To avoid noise effects, the double-ring method was used (64).

In vivo electrophysiological study. Dogs were anesthetized with morphine (2 mg/kg, SC)/alpha-chloralose (120 mg/kg, IV) and ventilated, and a median sternotomy was performed. Bipolar electrograms were recorded with bipolar Teflon-coated stainless steel electrodes sutured on the RA appendage (RAA). ARIs were measured as indices of APD (65), from the steepest portion of the initial atrial depolarization deflection to the end of the subsequent atrial repolarization signal. ARI alternans was defined by interbeat differences more than 5% over at least 6 successive beats, induced by a decremental S1-S1 pacing protocol (2 ms, 1.5 $\times$ diastolic threshold current stimuli). Starting at 300 ms, the BCL was decremented every 15 seconds in 10-ms steps until alternans occurred. Each pacing sequence was separated by at least 30 seconds to minimize the pacing memory. The BCL threshold for ARI alternans was defined as the maximal BCL that induced alternans. To assess AF vulnerability, an S1-S2 pacing protocol was applied at 8 discrete sites: RAA, left atrial appendage, and right and left atrial posterior walls, inferior walls, and Bachmann's bundles. AF vulnerability was defined as the percentage of atrial sites at which AF more than 1 second was reproducibly elicited by a single premature extrastimulus. To estimate mean AF duration in each dog, AF was induced with 1-second burst pacing applied 10 times (2 ms, 50 Hz, 4 $\times$ threshold current stimuli) in the RAA. Sustained AF (>20 minutes) was terminated by direct current cardioversion, and a 20-minute rest period was allowed for cardiac electrical recovery. If sustained AF was induced twice, no further AF induction was performed. After baseline data

were obtained, dantrolene (MilliporeSigma; 2.5 mg/kg, IV), an inhibitor of diastolic Ca^{2+} leak via RyR2 (13), was administered over 5 minutes, and measurements were repeated 20 minutes later.

Western blot analysis. ACM homogenates were prepared and protein concentrations determined with Amido black 10B (Sigma-Aldrich) or Bio-Rad Protein Assay Dye. Equivalent amounts of protein were fractionated on SDS-polyacrylamide gels and transferred to polyvinylidene difluoride membranes. Western blotting was performed with primary antibodies as previously described (66).

Immunoblotting was performed with primary antibodies against GAPDH (1:10,000; 10R-G109a, Fitzgerald Industries International), CSQ (1:2000; PA1-913, Thermo Fisher Scientific), calstabin2 (FKBP12.6, 1:1000; AF4174, R&D Systems), SERCA2a (1:5000; MAB2636, MilliporeSigma), total PLB (1:10,000; MA3 922, Thermo Fisher Scientific), Ser16- and Thr17-phosphorylated PLB (all 1:5000; A010-12 and A010-13, Badrilla), total RyR2 (1:5000; MA3-916, Thermo Fisher Scientific), and Ser2808- (1:5000; ab59225, Abcam) and Ser2814-phosphorylated RyR2 (1:5000; A010-31, Badrilla). For some studies, custom antibodies were used for Ser2808- (1:1000) and Ser2814-phosphorylated (1:200) RyR2. These antibodies were generated by Invitrogen, Thermo Fisher Scientific, with peptide sequences CNRTRRI pS QTSQ-AMIDE and CQTSQV pS VDAAH-AMIDE, respectively, in rabbits. For studies with custom antibodies, FKBP12.6 and CSQ, the GAPDH antibody used was from HyTest (5G4 6C5; 1:20,000). Protein bands were visualized with suitable near-infrared fluorophore dyes (IRDye, all 1:20,000, LI-COR Biosciences) or enhanced chemiluminescence and imaged with an Odyssey Infrared Imaging System (LI-COR Biosciences) or Bio-Rad Quantity One.

Statistics. Optical mapping, microfluometry, and confocal microscopy imaging data were processed with custom-made analysis software written in MATLAB (version 7.11, MathWorks). Statistical analysis was performed with IBM SPSS (version 20) and GraphPad Prism 5 software.

All summary data are expressed as mean ± SEM, unless otherwise specified. For variables that did not follow a normal distribution, we used the median and interquartile range (Q25–Q75) to represent central tendency and variability. A 2-tailed $P < 0.05$ was considered statistically significant. Continuous variables were compared with t tests (when only 2 groups were compared) or 2-way repeated measures ANOVA (when multiple groups, each with repeated measures were compared) or 1-way ANOVA (in the absence of repeated measures) followed by.Bonferroni's post hoc tests. Kolmogorov-Smirnov testing was used to check data normality. Data that did not satisfy criteria for normal distribution were compared with the nonparametric Kruskal-Wallis test followed by Dunn's post hoc test or by Wilcoxon's for matched single repeated-measures data. The incidence of SDA and AF was compared with 2×2 and 4×2 χ^2 tests.

Study approval. All animal handling procedures followed the National Institutes of Health guidelines and were approved by the comité de déontologie animale de l'Institut de Cardiologie de Montréal.

Author contributions

TL designed the study under supervision, conducted experiments with the help of FX and XYQ, and participated in data analysis and manuscript preparation; FX conducted experiments with TL and XYQ, participated in data analysis and manuscript preparation, wrote all signal analysis software, and ensured good functioning of the optical mapping system; XYQ helped with conducting of all single-cell experiments, as well as cell isolation; JX performed Western blot studies along with IAT; LV performed multiphoton confocal microscopy studies; IAT performed Western blot studies along with JX; DD supervised and funded Western blot studies and advised regarding the protocol and manuscript; and CH provided funding and supervision for TL. SN conceived the initial idea; worked closely with all coauthors to provide supervision at all points of experimentation, data analysis, and manuscript preparation; and provided funding for all experiments except Western blots.

Acknowledgments

Address correspondence to: Stanley Nattel, Montreal Heart Institute, 5000 rue Bélanger, Montréal H1T1C8, Québec, Canada. Phone: 514.376.3330; Email: stanley.nattel@icm-mhi.org.

1. Andrade J, Khairy P, Dobrev D, Nattel S. The clinical profile and pathophysiology of atrial fibrillation: relationships among clinical features, epidemiology, and mechanisms. *Circ Res*. 2014;114(9):1453–1468.

2. Heijman J, et al. The value of basic research insights into atrial fibrillation mechanisms as a guide to therapeutic innovation: a critical analysis. *Cardiovasc Res*. 2016;109(4):467–479.

3. Sun H, Gaspo R, Leblanc N, Nattel S. Cellular mechanisms of atrial contractile dysfunction caused by sustained atrial tachycardia. *Circulation*. 1998;98(7):719–727.

4. Sun H, Chartier D, Leblanc N, Nattel S. Intracellular calcium changes and tachycardia-induced contractile dysfunction in canine atrial myocytes. *Cardiovasc Res*. 2001;49(4):751–761.

5. Wang L, Myles RC, De Jesus NM, Ohlendorf AK, Bers DM, Ripplinger CM. Optical mapping of sarcoplasmic reticulum Ca2+ in the intact heart: ryanodine receptor refractoriness during alternans and fibrillation. *Circ Res*. 2014;114(9):1410–1421.

6. Hove-Madsen L, et al. Atrial fibrillation is associated with increased spontaneous calcium release from the sarcoplasmic reticulum in human atrial myocytes. *Circulation*. 2004;110(11):1358–1363.

7. Vest JA, et al. Defective cardiac ryanodine receptor regulation during atrial fibrillation. *Circulation*. 2005;111(16):2025–2032.

8. Voigt N, et al. Enhanced sarcoplasmic reticulum Ca2+ leak and increased Na+-Ca2+ exchanger function underlie delayed afterdepolarizations in patients with chronic atrial fibrillation. *Circulation*. 2012;125(17):2059–2070.

9. Voigt N, et al. Cellular and molecular mechanisms of atrial arrhythmogenesis in patients with paroxysmal atrial fibrillation. *Circulation*. 2014;129(2):145–156.

10. Xie W, Santulli G, Guo X, Gao M, Chen BX, Marks AR. Imaging atrial arrhythmic intracellular calcium in intact heart. *J Mol Cell Cardiol*. 2013;64:120–123.

11. Chang KC, Bayer JD, Trayanova NA. Disrupted calcium release as a mechanism for atrial alternans associated with human atrial fibrillation. *PLoS Comput Biol*. 2014;10(12):e1004011.

12. Saitoh H, Bailey JC, Surawicz B. Action potential duration alternans in dog Purkinje and ventricular muscle fibers. Further evidence in support of 2 different mechanisms. *Circulation*. 1989;80(5):1421–1431.

13. Kobayashi S, et al. Dantrolene, a therapeutic agent for malignant hyperthermia, markedly improves the function of failing cardiomyocytes by stabilizing interdomain interactions within the ryanodine receptor. *J Am Coll Cardiol*. 2009;53(21):1993–2005.

14. Porta M, et al. Single ryanodine receptor channel basis of caffeine's action on Ca2+ sparks. *Biophys J*. 2011;100(4):931–938.

15. Greiser M, et al. Tachycardia-induced silencing of subcellular Ca2+ signaling in atrial myocytes. *J Clin Invest*. 2014;124(11):4759–4772.

16. Yeh YH, et al. Calcium-handling abnormalities underlying atrial arrhythmogenesis and contractile dysfunction in dogs with congestive heart failure. *Circ Arrhythm Electrophysiol*. 2008;1(2):93–102.

17. Nishida K, et al. Mechanisms of atrial tachyarrhythmias associated with coronary artery occlusion in a chronic canine model. *Circulation*. 2011;123(2):137–146.

18. Chelu MG, et al. Calmodulin kinase II-mediated sarcoplasmic reticulum Ca2+ leak promotes atrial fibrillation in mice. *J Clin Invest*. 2009;119(7):1940–1951.

19. Avula UMR, et al. Atrial infarction-induced spontaneous focal discharges and atrial fibrillation in sheep: role of dantrolene-sensitive aberrant ryanodine receptor calcium release. *Circ Arrhythm Electrophysiol*. 2018;11(3):e005659.

20. Franz MR, Jamal SM, Narayan SM. The role of action potential alternans in the initiation of atrial fibrillation in humans: a review and future directions. *Europace*. 2012;14(suppl 5):v58–v64.

21. Pop T, Fleischmann D. Alternans in human atrial monophasic action potenial. *Br Heart J*. 1977;39(11):1273–1275.

22. Kim BS, et al. Action potential duration restitution kinetics in human atrial fibrillation. *J Am Coll Cardiol*. 2002;39(8):1329–1336.

23. Narayan SM, Franz MR, Clopton P, Pruvot EJ, Krummen DE. Repolarization alternans reveals vulnerability to human atrial fibrillation. *Circulation*. 2011;123(25):2922–2930.

24. Chang KC, Trayanova NA. Mechanisms of arrhythmogenesis related to calcium-driven alternans in a model of human atrial fibrillation. *Sci Rep*. 2016;6:36395.

25. Walker ML, Rosenbaum DS. Cellular alternans as mechanism of cardiac arrhythmogenesis. *Heart Rhythm*. 2005;2(12):1383–1386.

26. Wilson LD, Rosenbaum DS. Mechanisms of arrythmogenic cardiac alternans. *Europace*. 2007;9(suppl 6):vi77–vi82.

27. Hayashi H, et al. Dynamic origin of spatially discordant alternans in cardiac tissue. *Biophys J*. 2007;92(2):448–460.

28. Marks AR. Calcium cycling proteins and heart failure: mechanisms and therapeutics. *J Clin Invest*. 2013;123(1):46–52.

29. Wan X, Laurita KR, Pruvot EJ, Rosenbaum DS. Molecular correlates of repolarization alternans in cardiac myocytes. *J Mol Cell Cardiol*. 2005;39(3):419–428.

30. Cutler MJ, Wan X, Laurita KR, Hajjar RJ, Rosenbaum DS. Targeted SERCA2a gene expression identifies molecular mechanism and therapeutic target for arrhythmogenic cardiac alternans. *Circ Arrhythm Electrophysiol*. 2009;2(6):686–694.

31. Nassal MM, Wan X, Laurita KR, Cutler MJ. Atrial SERCA2a overexpression has no affect on cardiac alternans but promotes arrhythmogenic SR Ca2+ triggers. *PLoS One*. 2015;10(9):e0137359.

32. Sun B, et al. The cardiac ryanodine receptor, but not sarcoplasmic reticulum Ca^{2+}-ATPase, is a major determinant of Ca^{2+}alternans in intact mouse hearts. *J Biol Chem*. 2018;293(35):13650–13661.

33. Qu Z, Liu MB, Nivala M. A unified theory of calcium alternans in ventricular myocytes. *Sci Rep*. 2016;6:35625.

34. Rovetti R, Cui X, Garfinkel A, Weiss JN, Qu Z. Spark-induced sparks as a mechanism of intracellular calcium alternans in cardiac myocytes. *Circ Res*. 2010;106(10):1582–1591.

35. Belevych AE, et al. Redox modification of ryanodine receptors underlies calcium alternans in a canine model of sudden cardiac death. *Cardiovasc Res*. 2009;84(3):387–395.

36. Walther S, et al. Urocortin 2 stimulates nitric oxide production in ventricular myocytes via Akt- and PKA-mediated phosphory-

lation of eNOS at serine 1177. *Am J Physiol Heart Circ Physiol*. 2014;307(5):H689–H700.

37. Overend CL, O'Neill SC, Eisner DA. The effect of tetracaine on stimulated contractions, sarcoplasmic reticulum Ca2+ content and membrane current in isolated rat ventricular myocytes. *J Physiol (Lond)*. 1998;507(pt 3):759–769.

38. Faggioni M, Knollmann BC. Calsequestrin 2 and arrhythmias. *Am J Physiol Heart Circ Physiol*. 2012;302(6):H1250–H1260.

39. Chopra N, et al. Modest reductions of cardiac calsequestrin increase sarcoplasmic reticulum Ca2+ leak independent of luminal Ca2+ and trigger ventricular arrhythmias in mice. *Circ Res*. 2007;101(6):617–626.

40. Faggioni M, et al. Suppression of spontaneous ca elevations prevents atrial fibrillation in calsequestrin 2-null hearts. *Circ Arrhythm Electrophysiol*. 2014;7(2):313–320.

41. Zhong X, et al. Suppression of ryanodine receptor function prolongs Ca2+ release refractoriness and promotes cardiac alternans in intact hearts. *Biochem J*. 2016;473(21):3951–3964.

42. Yue L, Feng J, Gaspo R, Li GR, Wang Z, Nattel S. Ionic remodeling underlying action potential changes in a canine model of atrial fibrillation. *Circ Res*. 1997;81(4):512–525.

43. Nishida K, Michael G, Dobrev D, Nattel S. Animal models for atrial fibrillation: clinical insights and scientific opportunities. *Europace*. 2010;12(2):160–172.

44. Li D, Fareh S, Leung TK, Nattel S. Promotion of atrial fibrillation by heart failure in dogs: atrial remodeling of a different sort. *Circulation*. 1999;100(1):87–95.

45. Dobrev D, Voigt N, Wehrens XH. The ryanodine receptor channel as a molecular motif in atrial fibrillation: pathophysiological and therapeutic implications. *Cardiovasc Res*. 2011;89(4):734–743.

46. Heijman J, Guichard JB, Dobrev D, Nattel S. Translational challenges in atrial fibrillation. *Circ Res*. 2018;122(5):752–773.

47. Hartmann N, et al. Antiarrhythmic effects of dantrolene in human diseased cardiomyocytes. *Heart Rhythm*. 2017;14(3):412–419.

48. Chiang DY, et al. Loss of microRNA-106b-25 cluster promotes atrial fibrillation by enhancing ryanodine receptor type-2 and calcium release. *Circ Arrhythm Electrophysiol*. 2014;7(6):1214–1222.

49. Purohit A, et al. Oxidized Ca(2+)/calmodulin-dependent protein kinase II triggers atrial fibrillation. *Circulation*. 2013;128(16):1748–1757.

50. Coutu P, Chartier D, Nattel S. Comparison of Ca2+-handling properties of canine pulmonary vein and left atrial cardiomyocytes. *Am J Physiol Heart Circ Physiol*. 2006;291(5):H2290–H2300.

51. Brunello L, et al. Decreased RyR2 refractoriness determines myocardial synchronization of aberrant Ca2+ release in a genetic model of arrhythmia. *Proc Natl Acad Sci U S A*. 2013;110(25):10312–10317.

52. Cheng H, et al. Amplitude distribution of calcium sparks in confocal images: theory and studies with an automatic detection method. *Biophys J*. 1999;76(2):606–617.

53. Steele EM, Steele DS. Automated detection and analysis of Ca(2+) sparks in x-y image stacks using a thresholding algorithm implemented within the open-source image analysis platform ImageJ. *Biophys J*. 2014;106(3):566–576.

54. You YL, Kaveh M. Fourth-order partial differential equations for noise removal. *IEEE Trans Image Process*. 2000;9(10):1723–1730.

55. Rajan J, Kannan K, Kaimal M. An improved hybrid model for molecular image denoising. *J Math Imaging Vis*. 2008;31(1):73–79.

56. Benoist D, et al. Cardiac arrhythmia mechanisms in rats with heart failure induced by pulmonary hypertension. *Am J Physiol Heart Circ Physiol*. 2012;302(11):H2381–H2395.

57. Aguilar M, Xiong F, Qi XY, Comtois P, Nattel S. Potassium channel blockade enhances fibrillation-selective antiarrhythmic effects of optimized state-dependent sodium channel blockade. *Circulation*. 2015;132(23):2203–2211.

58. Jaimes R, Walton RD, Pasdois P, Bernus O, Efimov IR, Kay MW. A technical review of optical mapping of intracellular calcium within myocardial tissue. *Am J Physiol Heart Circ Physiol*. 2016;310(11):H1388–H1401.

59. Lang D, Sulkin M, Lou Q, Efimov IR. Optical mapping of action potentials and calcium transients in the mouse heart. *J Vis Exp*. 2011;null(55):3275.

60. Laughner JI, Ng FS, Sulkin MS, Arthur RM, Efimov IR. Processing and analysis of cardiac optical mapping data obtained with potentiometric dyes. *Am J Physiol Heart Circ Physiol*. 2012;303(7):H753–H765.

61. Nattel S, Xiong F, Aguilar M. Demystifying rotors and their place in clinical translation of atrial fibrillation mechanisms. *Nat Rev Cardiol*. 2017;14(9):509–520.

62. Bray MA, Wikswo JP. Considerations in phase plane analysis for nonstationary reentrant cardiac behavior. *Phys Rev E Stat Nonlin Soft Matter Phys*. 2002;65(5 pt 1):051902.

63. Zou R, Kneller J, Leon LJ, Nattel S. Development of a computer algorithm for the detection of phase singularities and initial application to analyze simulations of atrial fibrillation. *Chaos*. 2002;12(3):764–778.

64. Kuklik P, et al. Reconstruction of instantaneous phase of unipolar atrial contact electrogram using a concept of sinusoidal recomposition and Hilbert transform. *IEEE Trans Biomed Eng*. 2015;62(1):296–302.

65. Haws CW, Lux RL. Correlation between in vivo transmembrane action potential durations and activation-recovery intervals from electrograms. Effects of interventions that alter repolarization time. *Circulation*. 1990;81(1):281–288.

66. El-Armouche A, et al. Molecular determinants of altered Ca2+ handling in human chronic atrial fibrillation. *Circulation*. 2006;114(7):670–680.